

Unsupervised Protein-Ligand Binding Energy Prediction via Neural Euler’s Rotation Equation

Wengong Jin, Siranush Sarkizova, Xun Chen, Nir Hacohen, Caroline Uhler
Broad Institute of MIT and Harvard

Contact: wengong@csail.mit.edu

Abstract

Protein-ligand binding prediction is a fundamental problem in AI-driven drug discovery. Previous work focused on supervised learning methods for small molecules where binding affinity data is abundant, but it is hard to apply the same strategy to other ligand classes like antibodies where labelled data is limited. In this paper, we explore unsupervised approaches and reformulate binding energy prediction as a generative modeling task. Specifically, we train an energy-based model on a set of unlabelled protein-ligand complexes using SE(3) denoising score matching and interpret its log-likelihood as binding affinity. Our key contribution is a new equivariant rotation prediction network called Neural Euler’s Rotation Equations (NERE) for SE(3) score matching. It predicts a rotation by modeling the force and torque between protein and ligand atoms, where the force is defined as the gradient of an energy function with respect to atom coordinates. We evaluate NERE on protein-ligand and antibody-antigen binding affinity prediction benchmarks. Our model outperforms all unsupervised baselines (physics-based and statistical potentials) and matches supervised learning methods in the antibody case.

1. Introduction

One of the challenges in drug discovery is to design ligands (small molecules, antibodies, etc.) that bind to a target protein with high affinity. In recent years, a variety of protein-ligand binding prediction models have been developed for small molecule virtual screening [1–3]. They typically train neural networks on experimental binding data from PDB-Bind [4] and predict binding energy based on the 3D structure of protein-ligand complexes. However, it is difficult to apply the same strategy when binding affinity data is limited. For example, the largest binding affinity dataset for antibodies [5] has only about 600 data points (as opposed to 20000 for small molecules). Transfer learning from small

molecules to antibodies is also hard as their biochemical structures are very different.

Given the data scarcity challenge, we explore unsupervised learning approaches to binding energy prediction. Previous unsupervised methods are mostly based on physics, such as MM/GBSA [6] or Rosetta [7]. The basic idea is to hand-engineer an energy function so that crystal structures (stable conformations) have low energy. Nevertheless, these methods are either too simplistic or too expensive (relying on molecular dynamics) for large-scale virtual screening projects. Instead, we seek to learn an energy function by maximizing the log-likelihood (or minimizing the energy) of crystal structures in a training set. This *generative modeling* approach shares the same spirit as physics-based methods but uses more expressive architectures to capture all the nuances in the binding energy landscape. This approach is especially useful when there are few binding affinity data but many crystal structures.

In practice, we train our energy model via SE(3) denoising score matching (DSM) [8, 9] as maximum likelihood training is intractable. For each training example, we create a perturbed protein-ligand complex by randomly rotating/translating a ligand and ask our model to predict the rotation/translation noise. Though there are standard models [10] for predicting translations, predicting rotations in an equivariant manner remains an open challenge. The main contribution of this work is a new equivariant rotation prediction network called Neural Euler’s Rotation Equation (NERE). It first predicts atomic force defined as the gradient of an energy function with respect to atom coordinates. Next, it uses the force to calculate the torque between a protein and a ligand and infer ligand angular velocity based on its inertia matrix. Lastly, it outputs a rotation by taking the matrix exponential of learned angular velocity. Importantly, NERE can be plugged into any SE(3)-invariant network (a black box) and guarantees equivariance without specialized architectures.

We evaluate NERE on protein-ligand and antibody-antigen binding affinity benchmarks from PDBBind and Structural

Antibody Database (SAbDab) [5]. We compare NERE with unsupervised physics-based models (e.g., MM/GBSA and Rosetta) and statistical potentials like DrugScore₂₀₁₈ [11]. To simulate real-world virtual screening scenarios, we consider two settings where input complexes are either crystallized or predicted by a docking software. NERE outperforms all baselines in both cases and runs thousand times faster than MM/GBSA. For antibodies, it also matches the performance of supervised models trained on limited affinity data, which highlights the potential of unsupervised learning.

2. Related Work

Energy functions for small molecules fall into two categories: supervised and unsupervised learning. Supervised models are trained on binding affinity data from PDBBind [1–3, 12–15]. Their input is typically a protein-ligand 3D complex represented as a geometric graph, which is embedded into a latent representation by a neural network for affinity prediction. Unsupervised models are either based on physics or statistical potentials. For example, molecular mechanics Poisson–Boltzmann surface area (MM/PBSA) or generalized Born surface area (MM/GBSA) [6] calculate binding energy based on expensive molecular dynamics. Our work is closely related to statistical potentials including ASP [16], PMF [17], and DrugScore₂₀₁₈ [11]. They assign an interaction score (model parameters) for each atom pair based on their atom types and distance. These parameters are fit on a set of protein-ligand complexes based on maximum likelihood. In contrast, our model learns a neural network energy function that goes beyond pairwise interaction potentials and shows better performance.

Energy functions for antibodies and proteins are mostly physics-based potentials used in protein docking programs like ZRANK [18, 19], RosettaDock [7], PyDock [20], AP-PISA [21], and FIREDOCK [22]. They are typically weighted combinations of physics terms such as Van der Waals, electrostatics, salt bridges, and hydrophobic interactions. These weights are tuned so that crystal structures have lower energy than docked poses, but they are not trained on experimental binding data. Recently, Myung et al. [23] trained machine learning models on experimental binding affinity data from SAbDab, but they represent a binding interface using hand-engineered features. We reimplement their method using more advanced neural architectures as our baseline.

Equivariant rigid transformation. Motivated by docking, there has been a growing interest in predicting rigid transformations with equivariant neural networks. For instance, Ganea et al. [24], Stärk et al. [25] developed a graph matching network that first predicts a set of key points be-

tween a protein and a ligand, and then uses the Kabsch algorithm [26] to construct a rigid transformation in one shot. More recent work has turned to diffusion models that predict rigid transformations through an iterative process. As a pioneering work, Leach et al. [27] introduced isotropic Gaussian distributions $\mathcal{N}_{SO(3)}$ for SO(3) rotation group and developed a diffusion process based on rotation scaling and matrix exponential and logarithm maps. Later, Corso et al. [9] adopted $\mathcal{N}_{SO(3)}$ distribution and developed a diffusion model for small molecule docking. They predict rotations based on tensor field networks [28] instead of rotation scaling. Our method has two key differences with prior work. First, we always operate on angular velocity and never explicitly realize a rotation matrix, thus avoiding repeated matrix logarithm and exponentiation. Second, our method does not rely on spherical harmonics and can be plugged into any SE(3)-invariant encoder architectures for equivariant rotation prediction.

Energy-based models. Our model is an instance of energy-based models [29], which have recently been used for protein structure modeling [30, 31]. Our work is totally different from these methods because we focus on modeling binding energy (interaction between two proteins) rather than folding energy (single protein). As a result, our denoising score matching objective uses rigid transformation noise in SE(3) rather than Gaussian noise and we develop a new model for equivariant rotation score matching.

3. Neural Euler’s Rotation Equation

A protein-ligand complex is a geometric structure that involves a receptor protein and a ligand (a small molecule or an antibody). Each atom is associated with atom features \mathbf{a}_i and 3D coordinates \mathbf{x}_i . Thus, a protein-ligand complex is denoted as a tuple (\mathbf{A}, \mathbf{X}) , where $\mathbf{A} = [\mathbf{a}_1, \dots, \mathbf{a}_n]$ and $\mathbf{X} = [\mathbf{x}_1, \dots, \mathbf{x}_n]$ (column-wise concatenation). Our unsupervised binding energy prediction framework builds on SE(3) denoising score matching, where the key challenge is to predict rotation scores in an equivariant manner. In this section, we present Neural Euler’s Rotation Equation (NERE), an equivariant neural network for rotation prediction. To motivate our method, let us first review some basic concepts related to Euler’s rotation equations.

3.1. Euler’s Rotation Equations

In classical mechanics, Euler’s rotation equations is a first-order ordinary differential equation that describes the rotation of a rigid body. Suppose its current angular velocity is $\boldsymbol{\omega}$ and $\boldsymbol{\tau}$ is a torque applied to the ligand. The vector form of the Euler’s rotation equation is defined as

$$\mathbf{I}_N \frac{d\boldsymbol{\omega}}{dt} + \boldsymbol{\omega} \times (\mathbf{I}_N \boldsymbol{\omega}) = \boldsymbol{\tau}, \quad (1)$$

where $\mathbf{I}_N \in \mathbb{R}^{3 \times 3}$ is an inertia matrix that describes the mass distribution of a ligand and the torque needed for a desired angular acceleration. Importantly, the value of $\boldsymbol{\tau}$ and \mathbf{I}_N depends on the rotation center $\boldsymbol{\mu}$. Suppose all atoms have unit mass and each atom receives a force \mathbf{f}_i , the torque and inertia matrix are defined as follows

$$\boldsymbol{\tau} = \sum_{i \in \text{ligand}} (\mathbf{x}_i - \boldsymbol{\mu}) \times \mathbf{f}_i \quad (2)$$

$$\mathbf{I}_N = \sum_{i \in \text{ligand}} \|\mathbf{x}_i - \boldsymbol{\mu}\|^2 \mathbf{I} - (\mathbf{x}_i - \boldsymbol{\mu})(\mathbf{x}_i - \boldsymbol{\mu})^\top \quad (3)$$

In this paper, we choose $\boldsymbol{\mu}$ as the center of a ligand. Notice that when the ligand is static ($\boldsymbol{\omega} = 0$), Euler’s equation has a much simpler form $\mathbf{I}_N \frac{d\boldsymbol{\omega}}{dt} = \boldsymbol{\tau}$. We will use this simplified form for the rest of this work.

3.2. Force Layer

To predict a rotation using Euler’s rotation equations, we need to know the force \mathbf{f}_i of each atom. In this paper, we model this force term as the gradient $(\partial E / \partial \mathbf{x}_i)^\top$ of an energy function $E(\mathbf{A}, \mathbf{X})$. The advantage of this approach is that we can interpret the learned energy as binding affinity, which is very useful for virtual screening. By definition, the energy function must be differentiable with respect to \mathbf{X} and SE(3)-invariant. Thus, we adopt the frame averaging technique [32] so that E directly takes coordinates \mathbf{X} as input rather than a distance matrix. To be specific, our energy function is parameterized as follows

$$\mathbf{H} = \frac{1}{|\mathcal{G}|} \sum_{g_k \in \mathcal{G}} \phi_h(\mathbf{A}, g_k(\mathbf{X})) \quad (4)$$

$$E(\mathbf{A}, \mathbf{X}) = \sum_{i,j} \phi_o(\mathbf{h}_i, \mathbf{h}_j) \mathbb{I}[D_{ij} < d] \quad (5)$$

$$\mathbf{f}_i = \left(\frac{\partial E(\mathbf{A}, \mathbf{X})}{\partial \mathbf{x}_i} \right)^\top \quad (6)$$

where the encoder ϕ_h is a self-attention neural network [33] that learns atom representations $\mathbf{H} = [\mathbf{h}_1, \dots, \mathbf{h}_n]$ based on atom features \mathbf{A} and coordinates \mathbf{X} . In Eq.(4), the model first projects the coordinates \mathbf{X} onto a set of frames $\{g_k(\mathbf{X})\}$ defined in Puny et al. [32], encode each frame to hidden representations, and then average the frame representations to maintain SE(3) invariance. Finally, we compute the energy $E(\mathbf{A}, \mathbf{X})$ by modeling the pairwise potential $\phi_o(\mathbf{h}_i, \mathbf{h}_j)$ (scalar) between all atom pairs. The potential is calculated only for atoms within a distance threshold d because atomic interaction vanishes beyond certain distance.

Remark. We choose to model \mathbf{f}_i as the gradient $\partial E / \partial \mathbf{x}_i$ because we want to learn a binding energy function. For other applications like docking, \mathbf{f}_i can be the output of a

score network [8]. For example, we can predict \mathbf{f}_i using EGNN force layers [10]:

$$\mathbf{f}_i = \sum_j \mathbf{f}_{ij}, \quad \mathbf{f}_{ij} = \phi_x(\mathbf{h}_i, \mathbf{h}_j)(\mathbf{x}_i - \mathbf{x}_j) \quad (7)$$

where ϕ_x is a feed-forward neural network that takes the hidden representations $\mathbf{h}_i, \mathbf{h}_j$ and outputs the magnitude of the force (scalar) between points i and j . The force \mathbf{f}_{ij} follows the direction $\mathbf{x}_i - \mathbf{x}_j$. We leave the application of NERE to docking for future work.

3.3. Rotation Layer

As shown in Figure 1, NERE outputs a rotation based on the predicted forces in the following procedure

$$\boldsymbol{\omega} = C \mathbf{I}_N^{-1} \boldsymbol{\tau} = C \mathbf{I}_N^{-1} \sum_{i \in \text{ligand}} (\mathbf{x}_i - \boldsymbol{\mu}) \times \mathbf{f}_i \quad (8)$$

$$\mathbf{x}_i^{\text{new}} = \mathbf{x}_i + c_1 \boldsymbol{\omega} \times \mathbf{x}_i + c_2 \boldsymbol{\omega} \times (\boldsymbol{\omega} \times \mathbf{x}_i) \quad (9)$$

The rationale behind each equation is explained as follows. Eq.(8) calculates the torque $\boldsymbol{\tau}$ based on the predicted forces \mathbf{f}_{ij} and the resulting angular acceleration using the simplified Euler’s equation $\mathbf{I}_N \frac{d\boldsymbol{\omega}}{dt} = \boldsymbol{\tau}$. Assuming constant acceleration over a short time period C , the new angular velocity $\boldsymbol{\omega} = C \mathbf{I}_N^{-1} \boldsymbol{\tau}$. We note that calculating the inverse \mathbf{I}_N^{-1} is cheap because it is a constant 3×3 matrix.

Given the predicted angular velocity $\boldsymbol{\omega}$, its corresponding rotation matrix is defined by a matrix exponential map

$$\mathbf{R}_\omega = \exp(\mathbf{W}_\omega), \quad \mathbf{W}_\omega = \begin{pmatrix} 0 & -\omega_z & \omega_y \\ \omega_z & 0 & -\omega_x \\ -\omega_y & \omega_x & 0 \end{pmatrix}, \quad (10)$$

where $\boldsymbol{\omega} = (\omega_x, \omega_y, \omega_z)$ and \mathbf{W}_ω is an infinitesimal rotation matrix. Since \mathbf{W}_ω is a skew symmetric matrix, the matrix exponential has the following closed form

$$\mathbf{R}_\omega = \exp(\mathbf{W}_\omega) = \mathbf{I} + c_1 \mathbf{W}_\omega + c_2 \mathbf{W}_\omega^2 \quad (11)$$

$$c_1 = \frac{\sin \|\boldsymbol{\omega}\|}{\|\boldsymbol{\omega}\|}, \quad c_2 = \frac{1 - \cos \|\boldsymbol{\omega}\|}{\|\boldsymbol{\omega}\|^2} \quad (12)$$

Fortunately, we do not need to explicitly compute the matrix exponential \mathbf{R}_ω since \mathbf{W}_ω is the linear mapping of cross product, i.e. $\boldsymbol{\omega} \times \mathbf{r} = \mathbf{W}_\omega \mathbf{r}$. Therefore, applying the rotation matrix $\mathbf{R}_\omega \mathbf{x}_i$ is equivalent to Eq.(9) expressed in terms of cross products.

3.4. Analysis of Equivariance

Intuitively, NERE should be equivariant under SO(3) rotation group because it is derived from physics. We formally state this proposition as follows (proof in the appendix).

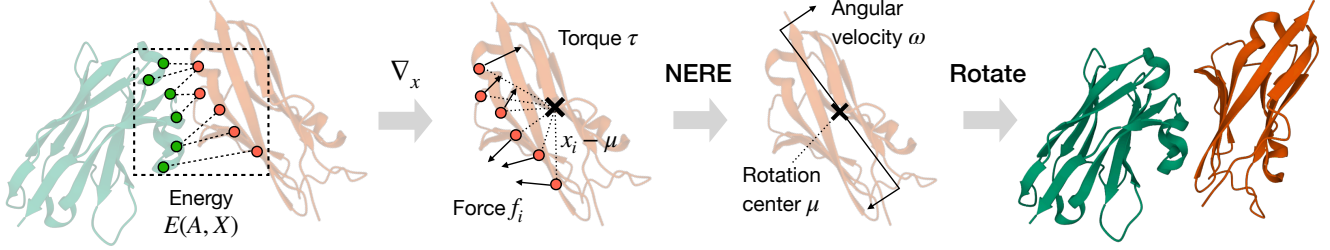


Figure 1. NERE predicts a rotation in three steps. It first calculates pairwise residue force based on the gradient $\mathbf{f}_i = (\partial E / \partial \mathbf{x})^\top$. It then predicts the corresponding torque and angular velocity by solving Euler’s rotation equation. Lastly, it converts the angular velocity vector to a rotation via matrix exponential map.

Proposition 1. Suppose we rotate a protein-ligand complex so that new coordinates become $\mathbf{x}'_i = \mathbf{R}\mathbf{x}_i$. The new force \mathbf{f}' , torque $\boldsymbol{\tau}'$, inertia matrix \mathbf{I}'_N , and angular velocity $\boldsymbol{\omega}'$ for the rotated complex are

$$\mathbf{f}'_i = \mathbf{R}\mathbf{f}_i, \boldsymbol{\tau}' = \mathbf{R}\boldsymbol{\tau}, \mathbf{I}'_N = \mathbf{R}\mathbf{I}_N\mathbf{R}^\top, \boldsymbol{\omega}' = \mathbf{R}\boldsymbol{\omega}$$

Therefore, we have $\mathbf{x}_i^{\text{new}'} = \mathbf{R}\mathbf{x}_i^{\text{new}}$.

Once we establish $\text{SO}(3)$ equivariance, it is easy to satisfy $\text{SE}(3)$ equivariance by first placing the rotation center at the origin ($\mathbf{x}_i \leftarrow \mathbf{x}_i - \boldsymbol{\mu}$), applying the predicted rotation via NERE, and then adding $\boldsymbol{\mu}$ back to each atom.

4. Unsupervised Binding Energy Prediction

In our unsupervised learning setup, our training set is a list of protein-ligand complexes without binding affinity labels. The basic idea behind our algorithm is that a crystal structure is the lowest energy state of a protein-ligand complex. Thus, we can learn a binding energy function $E(\mathbf{A}, \mathbf{X})$ by maximizing the likelihood of crystal structures in our training set. This approach is closely related to energy based models (EBMs) [29], where the likelihood of a data point $p(\mathbf{A}, \mathbf{X}) \propto \exp(-E(\mathbf{A}, \mathbf{X}))$. While maximum likelihood training is difficult for EBMs due to marginalization, recent work has successfully trained EBMs using denoising score matching (DSM) [8]. In this section, we describe 1) how to apply standard DSM to our task and 2) how to extend it to rigid transformation noise.

4.1. DSM with Gaussian Noise

Following standard DSM, we create a perturbed complex by adding Gaussian noise to ligand atom coordinates, i.e., $\tilde{\mathbf{X}} = \mathbf{X} + \boldsymbol{\epsilon}$, $\boldsymbol{\epsilon} \sim p(\boldsymbol{\epsilon}) = \mathcal{N}(0, \sigma^2 \mathbf{I})$. DSM objective tries to match the score of our model $\partial E / \partial \tilde{\mathbf{X}}$ and the score of the noise distribution $\nabla_{\boldsymbol{\epsilon}} \log p(\boldsymbol{\epsilon}) = -\boldsymbol{\epsilon} / \sigma^2$:

$$\ell_{\text{dsm}} = \mathbb{E}[\|\partial E(\mathbf{A}, \tilde{\mathbf{X}}) / \partial \tilde{\mathbf{X}} - \nabla_{\boldsymbol{\epsilon}} \log p(\boldsymbol{\epsilon})\|^2] \quad (13)$$

We note that $\partial E / \partial \tilde{\mathbf{X}}$ is the score of an actual energy function, which is different from standard score-based generative models that parameterize the score directly, leaving the energy function *implicit*. We choose to *explicitly* model the energy function because we want to use $E(\mathbf{A}, \mathbf{X})$ for binding energy prediction.

4.2. DSM with Rigid Transformation Noise

Nevertheless, adding Gaussian noise is not ideal for protein-ligand binding because it may create nonsensical conformations that violate physical constraints (e.g., an aromatic ring must be planar). A better solution is to create a perturbed complex $(\mathbf{A}, \tilde{\mathbf{X}})$ via random ligand rotation and translation, similar to molecular docking. To construct a random rotation, we sample an angular velocity vector $\boldsymbol{\omega}$ from $\mathcal{N}_{\text{SO}(3)}$, an isotropic Gaussian distribution over $\text{SO}(3)$ rotation group [27] with variance σ^2 . Each $\boldsymbol{\omega} \sim \mathcal{N}_{\text{SO}(3)}$ has the form $\boldsymbol{\omega} = \theta \hat{\boldsymbol{\omega}}$, where $\hat{\boldsymbol{\omega}}$ is a vector sampled uniformly from a unit sphere and $\theta \in [0, \pi]$ is a rotation angle with density

$$f(\theta) = \frac{1 - \cos \theta}{\pi} \sum_{l=0}^{\infty} (2l+1) e^{-l(l+1)\sigma^2} \frac{\sin((l+1/2)\theta)}{\sin(\theta/2)}$$

Likewise, we sample a random translation vector \mathbf{t} from a normal distribution $\mathbf{t} \sim \mathcal{N}(0, \sigma^2 \mathbf{I})$. Finally, we apply this rigid transformation to the ligand and compute its perturbed coordinates $\tilde{\mathbf{X}} = \mathbf{R}_{\boldsymbol{\omega}} \mathbf{X} + \mathbf{t}$, with $\mathbf{R}_{\boldsymbol{\omega}}$ defined in Eq.(10).

Under this formulation, DSM objective aims to match our score function $\partial E / \partial \tilde{\mathbf{X}}$ and the score of our noise distribution $\nabla_{\boldsymbol{\omega}} \log p(\boldsymbol{\omega})$, $\nabla_{\mathbf{t}} \log p(\mathbf{t})$. Both scores can be written in close forms. The translation vector \mathbf{t} follows a normal distribution, so $\nabla_{\mathbf{t}} \log p(\mathbf{t}) = -\mathbf{t} / \sigma^2$. As $\hat{\boldsymbol{\omega}}$ is sampled from a uniform distribution over a sphere whose density is constant, the density and score of $p(\boldsymbol{\omega})$ is

$$p(\boldsymbol{\omega}) \propto f(\theta), \quad \nabla_{\boldsymbol{\omega}} \log p(\boldsymbol{\omega}) = \nabla_{\theta} \log f(\theta) \cdot \hat{\boldsymbol{\omega}} \quad (14)$$

In practice, we calculate the density and score by precomputing truncated infinite series in $f(\theta)$. The main challenge,

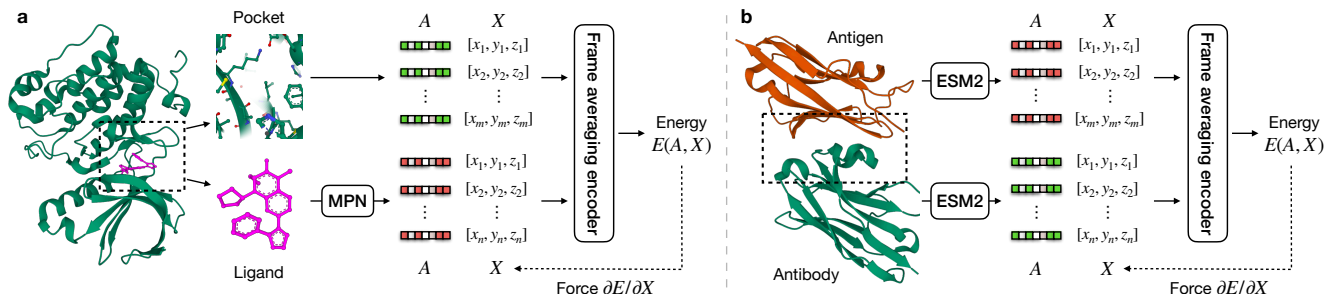


Figure 2. The architecture of $E(\mathbf{A}, \mathbf{X})$ for small molecules (left) and antibodies (right). For small molecules, the input is a binding pocket and a molecular graph encoded by a message passing network (MPN). For antibodies, the input contains antibody CDR residues and epitope residues, with residue features given by an ESM2 protein language model.

Algorithm 1 Training procedure (single data point)

Require: A training complex (\mathbf{A}, \mathbf{X}) .

- 1: Sample a noise level σ .
- 2: Sample rotation vector $\boldsymbol{\omega} \sim \mathcal{N}_{SO(3)}$ with variance σ^2
- 3: Sample translation vector $\mathbf{t} \sim \mathcal{N}(0, \sigma^2 \mathbf{I})$.
- 4: Perturb the coordinates $\tilde{\mathbf{X}}$ by applying rigid transformation $(\boldsymbol{\omega}, \mathbf{t})$ to the original complex.
- 5: Compute the score of energy function $(\tilde{\boldsymbol{\omega}}, \tilde{\mathbf{t}})$ based on its gradient $(\partial E / \partial \tilde{\mathbf{x}}_i)^\top$ and NERE.
- 6: Minimize DSM objective ℓ_{dsm} .

however, is that our score function $\partial E / \partial \tilde{\mathbf{X}}$ is defined over atom coordinates, which is not directly comparable with $\nabla_{\boldsymbol{\omega}} \log p(\boldsymbol{\omega})$, $\nabla_{\mathbf{t}} \log p(\mathbf{t})$ as they have different dimensions. To address this issue, we propose to project $\partial E / \partial \tilde{\mathbf{X}}$ to angular velocity $\tilde{\boldsymbol{\omega}}$ via NERE (see Eq.(8)) and perform score matching in the rotation and translation space:

$$\ell_{\text{dsm}} = \mathbb{E}[\|\tilde{\boldsymbol{\omega}} - \nabla_{\boldsymbol{\omega}} \log p(\boldsymbol{\omega})\|^2 + \|\tilde{\mathbf{t}} - \nabla_{\mathbf{t}} \log p(\mathbf{t})\|^2]$$

$$\tilde{\boldsymbol{\omega}} = C \mathbf{I}_N^{-1} \boldsymbol{\tau}, \quad \tilde{\mathbf{t}} = \frac{1}{n} \sum_i \mathbf{f}_i$$

Here, $\boldsymbol{\tau}, \mathbf{f}_i$ are functions of $\partial E / \partial \tilde{\mathbf{X}}$ and $\tilde{\boldsymbol{\omega}}, \tilde{\mathbf{t}}$ are the rotation and translation score. In our experiments, we find this ‘‘projected’’ score matching objective to be quite effective and we leave its theoretical analysis to future work. The training procedure is summarized in Algorithm 1.

4.3. Applications to Small Molecules and Antibodies

So far, we have described our method in generic terms. In this section, we specify atom features \mathbf{A} and model architecture tailored to small molecules and antibodies.

Small molecules. When the ligand is a small molecule, the input to our model is a protein-ligand complex where the protein is cropped to its binding pocket (residues within 10Å from the ligand). The model architecture is illustrated in Figure 2a. On the protein side, each atom in the bind-

ing pocket is represented by a one-hot encoding of its atom name (C_α , C_β , N, O, etc.). We consider all backbone and side-chain atoms. On the ligand side, the atom features \mathbf{A} are learned by a message passing network (MPN) [34] based on a ligand molecular graph. We jointly train the MPN and energy function using the DSM objective.

Antibodies. When the ligand is an antibody drug, the input to our model is an antibody-antigen binding interface. The binding interface is composed of residues in the antibody complementarity-determining region (CDR) of both heavy and light chains and top 50 antigen residues (epitope) closest to the CDR. The model architecture is depicted in Figure 2b. Different from the small molecule case, we only consider C_α atoms of each antibody/antigen residue. Each residue is represented by a 2560 dimensional pre-trained ESM-2 embedding [35]. For computational efficiency, we do not fine-tune ESM-2 during training.

5. Experiments

We evaluate our model on two drug discovery applications: protein-ligand binding and antibody-antigen binding affinity prediction. The experimental setup is described as follows.

5.1. Protein-Ligand Binding

Data. Our training data comes from the refined subset of PDBbind v2020 database, which has 5237 protein-ligand complexes with binding affinity labels converted into log scale. Our test set is the PDBbind core set (285 complexes). Our validation set has 363 complexes randomly sampled from PDBbind by Stärk et al. [25] (excluding any test cases). Our training set has 4806 complexes after removing all ligands overlapping with the test set.

Metric. We report the Pearson correlation coefficient between true binding affinity and model prediction $E(\mathbf{A}, \mathbf{X})$. We do not report root mean square error (RMSE) because

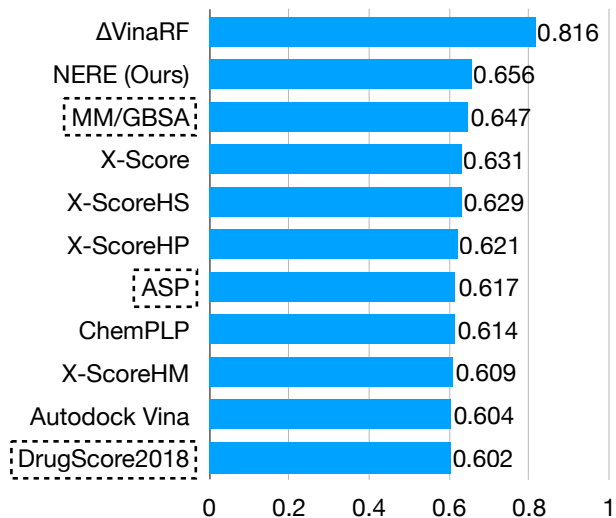


Figure 3. Pearson correlation on the CASF test set (crystal structures). Unsupervised methods are marked with dash lines. We only report top 10 methods in CASF due to limited space.

our model does not predict absolute affinity values. In fact, shifting $E(\mathbf{A}, \mathbf{X})$ by any constant will be equally optimal under the DSM objective. We run our model with five different random seeds and report their average.

Baselines. Comparative assessment of scoring functions (CASF challenge) [4] has evaluated more than 30 binding affinity prediction methods on the PDBbind core test set. Majority of them were supervised models because they are trained on binding affinity labels in PDBbind or other databases. Due to limited space, we only report top 10 methods ranked by their performance. We mainly compare with three unsupervised methods that are labeled by CASF as knowledge-based potential or physics-based function:¹

- DrugScore2018 [11] and ASP [16] are statistical potentials learned from crystal structures based on maximum likelihood objective.
- MM/GBSA [6, 36] is a physics-based method that calculates protein-ligand binding energy based on molecular dynamics. It is computationally expensive but more accurate than statistical potentials (approximate run-time: 1-2 hour per complex on a 64-core CPU server with parallelization).

Results (crystal structures). In our first experiment, we follow the CASF challenge setting and evaluate all methods using the crystal structure of protein-ligand complexes. Our results are shown in Figure 3, where the baseline re-

¹We do not consider models developed after CASF such as TANKBind [3] since they are supervised. We also exclude buried solvent accessible surface area (Δ SAS) baseline because we could not reproduce its result reported in CASF.

	Crystal	Vina
DrugScore2018	0.602	0.540
MM/GBSA	0.647	0.629
NERE (ours)	0.656 _{.012}	0.651 _{.011}
- rotation only	0.622 _{.015}	0.621 _{.014}
- translation only	0.266 _{.315}	0.274 _{.306}
- standard DSM	0.638 _{0.017}	0.632 _{.016}

Table 1. Pearson correlation on the CASF test set (both crystal and docked structures). Standard deviation is shown in subscript. Here we focus on the comparison with unsupervised baselines.

sults are copied from Su et al. [4] and Jones et al. [36]. Our model outperforms all baselines except Δ VinaRF, which is a supervised model trained on binding affinity data in PDBbind. Importantly, our model is much more scalable than MM/GBSA (10ms v.s. 1hr per complex). Overall, these results suggest that it is possible to learn binding free energy in a pure data-driven manner without physical knowledge.

Results (docked structures). Previous evaluation considers an idealistic setting because crystal structures are not available in real-world virtual screening projects. To this end, we use AutoDock Vina [37] to dock each ligand in the test set to its binding pocket and evaluate all methods on docked protein-ligand complexes. We specify binding pocket location by constructing a docking grid (size=20Å) around the binding pocket. In terms of baseline, here we focus on comparison with unsupervised methods (DrugScore2018 and MM/GBSA). We could not evaluate ASP because it is proprietary. The result of MM/GBSA on Vina poses are copied from Jones et al. [36].

Our results are summarized in Table 1. NERE consistently outperforms the baselines in this setting. Its performance on Vina poses is quite close to the crystal structure setting because docking error is relatively low (median test RMSD 3.55). Our model is also less sensitive to docking error than the baselines. Overall, these results suggest that NERE is suitable for binding energy calculation in real-world virtual screening projects.

5.2. Antibody-Antigen Binding

Data. Our training and test data come from the Structural Antibody Database (SAbDab) [5]. It contains 4883 antibody-antigen complexes after removing duplicates and structures without antigens, among which 566 instances have binding affinity labels (ΔG) and used as our test set. Our training set has 3416 complexes after removing antigen/antibody sequences overlapping with the test set (over 99% sequence similarity). Our validation set comes from Myung et al. [23], which has 197 complexes after removing

instances appeared in the test set.

Baselines. Following Guest et al. [38], we compare our method with a variety of physic-based potentials, including ZRANK, ZRANK2 [18, 19], RosettaDock [7], PyDock [20], SIPPER [39], AP_PISA [21], CP_PIE [40], FIREDOCK, and FIREDOCK_AB [22]. They are implemented in the CCharPPI web server [41].

We also consider a supervised regression model trained on limited binding affinity data in our validation set (our training set does not have affinity labels). It has the same encoder architecture as NERE. We train both NERE and this supervised neural network (NN) with five different random seeds and report their average performance. For supervised NN, we randomly select half of the validation set for training and the other half for validation.

Results (Crystal structure). Similar to protein-ligand binding, we first evaluate all models on crystal structures and report the Pearson correlation coefficient between true and predicted binding energy. As shown in Table 2, our model outperforms existing physics-based potentials and supervised NN despite not using any binding affinity data. The performance of supervised NN is quite unstable (large standard deviation) as the training data is limited. In this particular case, training with unlabelled data (≈ 3000 complexes) leads to more effective and stable models.

Results (Docked structure). In our second experiment, the input complexes are predicted by a docking software to emulate a more realistic scenario. We use a common docking program called ZDOCK [42] to predict the structure of all antibody-antigen complexes in the test set. Our model still outperforms all the baselines in this challenging setting. Yet, all models yield a much lower performance due to considerable docking error (test median RMSD is 19.4). Both NERE and supervised NN have similar performance given that supervised NN has a large standard deviation, but NERE is more sensitive to docking error. In summary, docking accuracy is crucial to binding energy prediction and we need to either improve docking accuracy or the robustness of binding energy predictors.

5.3. Ablation Study and Visualization

Ablation studies. We first compare SE(3) DSM with standard DSM, which perturbs each atom with a Gaussian noise rather than rotating the ligand as a rigid body. We find that SE(3) DSM achieves better performance especially in the docked setting (Table 1: 0.651/0.632; Table 2: 0.234/0.207). Indeed, adding Gaussian noise is undesirable as it deforms the ligand shape and creates invalid conformations. In addition, we run NERE by keeping only the rotation or translation score matching term in our training objective ℓ_{dsm} . As shown in Table 1 and 2), incorporat-

	Crystal	ZDOCK
ZRANK	0.318	0.163
ZRANK2	0.176	0.151
RosettaDOCK	0.064	0.025
PYDOCK	0.248	0.164
SIPPER	-0.138	0.003
AP_PISA	0.323	0.144
FIREDOCK	0.101	-0.052
FIREDOCK_AB	0.199	0.042
CP_PIE	0.234	0.120
NERE (ours)	0.340 _{.029}	0.234 _{.040}
- rotation only	0.303 _{.026}	0.194 _{.066}
- translation only	0.312 _{.038}	0.178 _{.054}
- standard DSM	0.335 _{.038}	0.207 _{.037}
Supervised NN	0.295 _{.098}	0.258 _{.100}

Table 2. Pearson correlation on SABDab test set (both crystal and docked structures). Standard deviation is only shown for NERE because baseline models are deterministic.

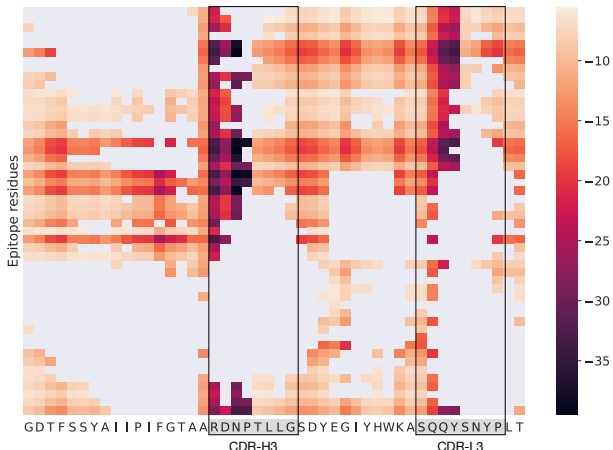


Figure 4. The heat map of our learned energy function. Each entry represent the binding energy between residues (i, j) (the darker the stronger). An entry is left blank (grey) if their distance $D_{ij} > d$. Our model correctly puts more attention to CDR-H3/L3 residues.

ing both terms gives the best performance, i.e., considering both degree of freedom is crucial to unsupervised binding prediction.

Visualizing interaction energy. Next, we investigate the contribution of different residues to predicted binding energy. Figure 4 is a heat map of an antibody-antigen complex, where each row and column represent an epitope residue and an antibody CDR residue, respectively. Each entry in the heat map is the energy between two residue (re-

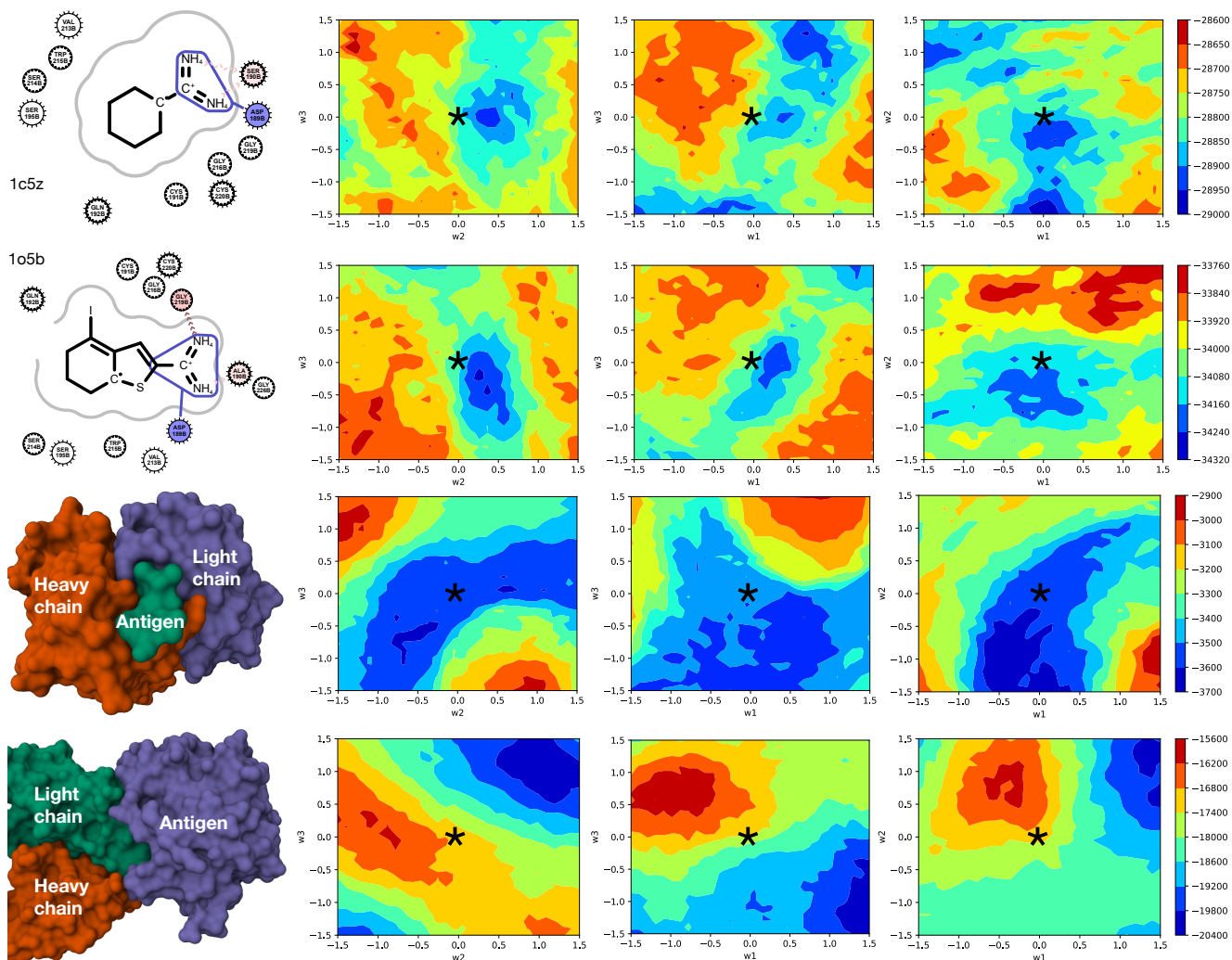


Figure 5. Visualizing learned energy landscape for small molecules (row 1-2) and antibodies (row 3-4). We perform a grid search of ligand rotation angles $\omega = [\omega_1, \omega_2, \omega_3]$ and plot the predicted energy as 2D contour plots with one of the axis ω_i fixed. The crystal structure is at the origin (marked with *) and supposed to be the local minima of the energy landscape.

call that $E(\mathbf{A}, \mathbf{X})$ is a summation $\sum_{i,j} \phi_o(\mathbf{h}_i, \mathbf{h}_j) \mathbb{I}[D_{ij} < d]$. An entry is left blank if the distance $D_{i,j} > d$, where $d = 20\text{\AA}$. Interestingly, we find that the model pays the most attention to CDR-H3 and CDR-L3 residues. In most test cases, their energy is much lower than other CDR residues. This agrees with the domain knowledge that CDR-H3 and CDR-L3 residues is the major component for binding.

Visualizing energy landscape. Lastly, we study how the learned energy changes with respect to ligand orientations. Given an input complex, we perform a grid search of ligand rotation angles $\omega = [\omega_1, \omega_2, \omega_3]$ and plot the predicted energy for each pose. As 3D contour plot is hard to visualize, we decompose it into three 2D contour plots by fixing one of the three axis ($\omega_1, \omega_2, \omega_3$) to zero. Ideally, the crys-

tal structure ($\omega = [0, 0, 0]$) should be the local minimum because it is physically the most stable conformation. Figure 5 show contour plots for small molecules and antibody-antigen complexes. For small molecules and peptide antigens (row 1-3), their crystal structures are located relatively near the local minimum. For general antigens, the learned energy landscape often fails to recognize crystal structures as local minima (row 4). Indeed, antibody-antigen binding has much greater flexibility than small molecules in terms of binding conformations, as indicated by their docking RMSD (19.4 vs 3.55). Overall, our model still has much room for improvement. Enhancing the energy landscape quality may improve its correlation with experimental binding affinity.

6. Discussion

In this paper, we develop a generative model for unsupervised binding energy prediction and an equivariant neural network for rotation prediction. The energy-based model is trained under SE(3) denoising score matching where rotation score is predicted by Neural Euler’s Rotation Equation. Our results indicate that inferred log-likelihood correlates with experimental binding affinity for small molecules and antibodies. Indeed, there remain many ways to improve our method. For example, we haven’t incorporated side chain structures or rotatable bonds in DSM, which is crucial for protein binding. We also need to improve the robustness of binding predictors since they are susceptible to docking errors. We envision that NERE is applicable to a variety of binding problems in structural biology, such as peptide-HLA, TCR-pMHC, and protein-RNA interaction.

Acknowledgement

We want to thank Divya Nori and Jeremy Wohlwend for their valuable feedback on the manuscript. Funding to support this research was provided by the Eric and Wendy Schmidt Center at Broad Institute.

References

- [1] Lifan Chen, Xiaoqin Tan, Dingyan Wang, Feisheng Zhong, Xiaohong Liu, Tianbiao Yang, Xiaomin Luo, Kaixian Chen, Hualiang Jiang, and Mingyue Zheng. TransformerCPI: improving compound–protein interaction prediction by sequence-based deep learning with self-attention mechanism and label reversal experiments. *Bioinformatics*, 36(16):4406–4414, 2020. 1, 2
- [2] Vignesh Ram Somnath, Charlotte Bunne, and Andreas Krause. Multi-scale representation learning on proteins. *Advances in Neural Information Processing Systems*, 34:25244–25255, 2021.
- [3] Wei Lu, Qifeng Wu, Jixian Zhang, Jiahua Rao, Chengtao Li, and Shuangjia Zheng. Tankbind: Trigonometry-aware neural networks for drug-protein binding structure prediction. *bioRxiv*, 2022. 1, 2, 6
- [4] Minyi Su, Qifan Yang, Yu Du, Guoqin Feng, Zhihai Liu, Yan Li, and Renxiao Wang. Comparative assessment of scoring functions: the casf-2016 update. *Journal of chemical information and modeling*, 59(2):895–913, 2018. 1, 6
- [5] Constantin Schneider, Matthew IJ Raybould, and Charlotte M Deane. Sabdab in the age of biotherapeutics: updates including sabdab-nano, the nanobody structure tracker. *Nucleic acids research*, 50(D1):D1368–D1372, 2022. 1, 2, 6
- [6] Bill R Miller III, T Dwight McGee Jr, Jason M Swails, Nadine Homeyer, Holger Gohlke, and Adrian E Roitberg. Mmpbsa.py: an efficient program for end-state free energy calculations. *Journal of chemical theory and computation*, 8(9):3314–3321, 2012. 1, 2, 6
- [7] Rebecca F Alford, Andrew Leaver-Fay, Jeliasko R Jeliaskov, Matthew J O’Meara, Frank P DiMaio, Hahnbeom Park, Maxim V Shapovalov, P Douglas Renfrew, Vikram K Mulligan, Kalli Kappel, et al. The rosetta all-atom energy function for macromolecular modeling and design. *Journal of chemical theory and computation*, 13(6):3031–3048, 2017. 1, 2, 7
- [8] Yang Song and Stefano Ermon. Generative modeling by estimating gradients of the data distribution. *Advances in Neural Information Processing Systems*, 32, 2019. 1, 3, 4
- [9] Gabriele Corso, Hannes Stärk, Bowen Jing, Regina Barzilay, and Tommi Jaakkola. Diffdock: Diffusion steps, twists, and turns for molecular docking. *arXiv preprint arXiv:2210.01776*, 2022. 1, 2
- [10] Victor Garcia Satorras, Emiel Hoogeboom, and Max Welling. E(n) equivariant graph neural networks. In *International conference on machine learning*, pages 9323–9332. PMLR, 2021. 1, 3
- [11] Jonas Dittrich, Denis Schmidt, Christopher Pfleger, and Holger Gohlke. Converging a knowledge-based scoring function: Drugscore2018. *Journal of chemical information and modeling*, 59(1):509–521, 2018. 2, 6
- [12] Matthew Ragoza, Joshua Hochuli, Elisa Idrobo, Jocelyn Sunseri, and David Ryan Koes. Protein–ligand scoring with convolutional neural networks. *Journal of chemical information and modeling*, 57(4):942–957, 2017. 2
- [13] José Jiménez, Miha Skalic, Gerard Martinez-Rosell, and Gianni De Fabritiis. K-deep: protein–ligand absolute binding affinity prediction via 3d-convolutional neural networks. *Journal of chemical information and modeling*, 58(2):287–296, 2018.
- [14] Penglei Wang, Shuangjia Zheng, Yize Jiang, Chengtao Li, Junhong Liu, Chang Wen, Atanas Patronov, Dahong Qian, Hongming Chen, and Yuedong Yang. Structure-aware multimodal deep learning for drug–protein interaction prediction. *Journal of chemical information and modeling*, 62(5):1308–1317, 2022.

- [15] Seokhyun Moon, Wonho Zhung, Soojung Yang, Jaechang Lim, and Woo Youn Kim. Pignet: a physics-informed deep learning model toward generalized drug–target interaction predictions. *Chemical Science*, 13(13):3661–3673, 2022. 2
- [16] Wijnand TM Mooij and Marcel L Verdonk. General and targeted statistical potentials for protein–ligand interactions. *Proteins: Structure, Function, and Bioinformatics*, 61(2):272–287, 2005. 2, 6
- [17] Ingo Muegge. Pmf scoring revisited. *Journal of medicinal chemistry*, 49(20):5895–5902, 2006. 2
- [18] Brian Pierce and Zhiping Weng. Zrank: reranking protein docking predictions with an optimized energy function. *Proteins: Structure, Function, and Bioinformatics*, 67(4):1078–1086, 2007. 2, 7
- [19] Brian Pierce and Zhiping Weng. A combination of rescoring and refinement significantly improves protein docking performance. *Proteins: Structure, Function, and Bioinformatics*, 72(1):270–279, 2008. 2, 7
- [20] Solène Grosdidier, Carles Pons, Albert Solernou, and Juan Fernández-Recio. Prediction and scoring of docking poses with pydock. *Proteins: Structure, Function, and Bioinformatics*, 69(4):852–858, 2007. 2, 7
- [21] Shruthi Viswanath, DVS Ravikant, and Ron Elber. Improving ranking of models for protein complexes with side chain modeling and atomic potentials. *Proteins: Structure, Function, and Bioinformatics*, 81(4):592–606, 2013. 2, 7
- [22] Nelly Andrusier, Ruth Nussinov, and Haim J Wolfson. Firedock: fast interaction refinement in molecular docking. *Proteins: Structure, Function, and Bioinformatics*, 69(1):139–159, 2007. 2, 7
- [23] Yoochan Myung, Douglas EV Pires, and David B Ascher. Csm-ab: graph-based antibody–antigen binding affinity prediction and docking scoring function. *Bioinformatics*, 38(4):1141–1143, 2022. 2, 6
- [24] Octavian-Eugen Ganea, Xinyuan Huang, Charlotte Bunne, Yatao Bian, Regina Barzilay, Tommi Jaakkola, and Andreas Krause. Independent SE(3)-equivariant models for end-to-end rigid protein docking. *arXiv preprint arXiv:2111.07786*, 2021. 2
- [25] Hannes Stärk, Octavian Ganea, Lagnajit Pattanaik, Regina Barzilay, and Tommi Jaakkola. Equibind: Geometric deep learning for drug binding structure prediction. In *International Conference on Machine Learning*, pages 20503–20521. PMLR, 2022. 2, 5
- [26] Wolfgang Kabsch. A solution for the best rotation to relate two sets of vectors. *Acta Crystallographica Section A: Crystal Physics, Diffraction, Theoretical and General Crystallography*, 32(5):922–923, 1976. 2
- [27] Adam Leach, Sebastian M Schmon, Matteo T Degiacomi, and Chris G Willcocks. Denoising diffusion probabilistic models on so (3) for rotational alignment. In *ICLR 2022 Workshop on Geometrical and Topological Representation Learning*, 2022. 2, 4
- [28] Nathaniel Thomas, Tess Smidt, Steven Kearnes, Lussann Yang, Li Li, Kai Kohlhoff, and Patrick Riley. Tensor field networks: Rotation-and translation-equivariant neural networks for 3d point clouds. *arXiv preprint arXiv:1802.08219*, 2018. 2
- [29] Yann LeCun, Sumit Chopra, Raia Hadsell, M Ranzato, and Fugie Huang. A tutorial on energy-based learning. *Predicting structured data*, 1(0), 2006. 2, 4
- [30] Yilun Du, Joshua Meier, Jerry Ma, Rob Fergus, and Alexander Rives. Energy-based models for atomic-resolution protein conformations. *International Conference on Learning Representations*, 2020. 2
- [31] Jiaxiang Wu, Shitong Luo, Tao Shen, Haidong Lan, Sheng Wang, and Junzhou Huang. Ebm-fold: fully-differentiable protein folding powered by energy-based models. *arXiv preprint arXiv:2105.04771*, 2021. 2
- [32] Omri Puny, Matan Atzmon, Heli Ben-Hamu, Edward J Smith, Ishan Misra, Aditya Grover, and Yaron Lipman. Frame averaging for invariant and equivariant network design. *arXiv preprint arXiv:2110.03336*, 2021. 3
- [33] Tao Lei. When attention meets fast recurrence: Training language models with reduced compute. *arXiv preprint arXiv:2102.12459*, 2021. 3
- [34] Kevin Yang, Kyle Swanson, Wengong Jin, Connor Coley, Philipp Eiden, Hua Gao, Angel Guzman-Perez, Timothy Hopper, Brian Kelley, Miriam Mathea, et al. Analyzing learned molecular representations for property prediction. *Journal of chemical information and modeling*, 59(8):3370–3388, 2019. 5, 12
- [35] Zeming Lin, Halil Akin, Roshan Rao, Brian Hie, Zhongkai Zhu, Wenting Lu, Allan dos Santos Costa, Maryam Fazel-Zarandi, Tom Sercu, Sal Candido, et al. Language models of protein sequences at the scale of evolution enable accurate structure prediction. *bioRxiv*, 2022. 5

- [36] Derek Jones, Hyojin Kim, Xiaohua Zhang, Adam Zemla, Garrett Stevenson, WF Drew Bennett, Daniel Kirshner, Sergio E Wong, Felice C Lightstone, and Jonathan E Allen. Improved protein–ligand binding affinity prediction with structure-based deep fusion inference. *Journal of chemical information and modeling*, 61(4):1583–1592, 2021. 6
- [37] Jerome Eberhardt, Diogo Santos-Martins, Andreas F Tillack, and Stefano Forli. Autodock vina 1.2.0: New docking methods, expanded force field, and python bindings. *Journal of Chemical Information and Modeling*, 61(8):3891–3898, 2021. 6
- [38] Johnathan D Guest, Thom Vreven, Jing Zhou, Iain Moal, Jeliasko R Jeliaskov, Jeffrey J Gray, Zhiping Weng, and Brian G Pierce. An expanded benchmark for antibody-antigen docking and affinity prediction reveals insights into antibody recognition determinants. *Structure*, 29(6):606–621, 2021. 7
- [39] Carles Pons, David Talavera, Xavier De La Cruz, Modesto Orozco, and Juan Fernandez-Recio. Scoring by intermolecular pairwise propensities of exposed residues (sipper): a new efficient potential for protein-protein docking. *Journal of chemical information and modeling*, 51(2):370–377, 2011. 7
- [40] DVS Ravikant and Ron Elber. Pie—efficient filters and coarse grained potentials for unbound protein–protein docking. *Proteins: Structure, Function, and Bioinformatics*, 78(2):400–419, 2010. 7
- [41] Iain H Moal, Brian Jiménez-García, and Juan Fernández-Recio. Ccharppi web server: computational characterization of protein–protein interactions from structure. *Bioinformatics*, 31(1):123–125, 2015. 7
- [42] Brian G Pierce, Kevin Wiehe, Howook Hwang, Bong-Hyun Kim, Thom Vreven, and Zhiping Weng. Zdock server: interactive docking prediction of protein–protein complexes and symmetric multimers. *Bioinformatics*, 30(12):1771–1773, 2014. 7

A. NERE Rotational Equivariance

Proposition 1. Suppose we rotate a protein-ligand complex so that new coordinates become $\mathbf{x}'_i = \mathbf{R}\mathbf{x}_i$. The new force \mathbf{f}' , torque $\boldsymbol{\tau}'$, inertia matrix \mathbf{I}'_N , and angular velocity $\boldsymbol{\omega}'$ under the rotated complex are

$$\mathbf{f}'_i = \mathbf{R}\mathbf{f}_i, \boldsymbol{\tau}' = \mathbf{R}\boldsymbol{\tau}, \mathbf{I}'_N = \mathbf{R}\mathbf{I}_N\mathbf{R}^\top, \boldsymbol{\omega}' = \mathbf{R}\boldsymbol{\omega},$$

Therefore, we have $\mathbf{x}_i^{\text{new}'} = \mathbf{R}\mathbf{x}_i^{\text{new}}$.

Proof. After rotating the whole complex, the energy function $E(\mathbf{A}, \mathbf{X}') = E(\mathbf{A}, \mathbf{X})$ since the encoder is SE(3)-invariant. Given that $\mathbf{x}_i = \mathbf{R}^\top \mathbf{x}'_i$ and $\partial \mathbf{x}_i / \partial \mathbf{x}'_i = \mathbf{R}^\top$, the new force becomes

$$\begin{aligned} \mathbf{f}'_i &= \left(\frac{\partial E(\mathbf{A}, \mathbf{X}')}{\partial \mathbf{x}'_i} \right)^\top = \left(\frac{\partial E(\mathbf{A}, \mathbf{X})}{\partial \mathbf{x}_i} \frac{\partial \mathbf{x}_i}{\partial \mathbf{x}'_i} \right)^\top \\ &= \left(\frac{\partial \mathbf{x}_i}{\partial \mathbf{x}'_i} \right)^\top \mathbf{f}_i = \mathbf{R}\mathbf{f}_i \end{aligned}$$

Based on the definition of torque and the fact that cross products satisfy $\mathbf{R}\mathbf{x} \times \mathbf{R}\mathbf{y} = \mathbf{R}(\mathbf{x} \times \mathbf{y})$, we have

$$\begin{aligned} \boldsymbol{\tau}' &= \sum_i (\mathbf{x}'_i - \boldsymbol{\mu}') \times \mathbf{f}'_i = \sum_i (\mathbf{R}\mathbf{x}_i - \mathbf{R}\boldsymbol{\mu}) \times \mathbf{R}\mathbf{f}_i \\ &= \mathbf{R} \sum_i (\mathbf{x}_i - \boldsymbol{\mu}) \times \mathbf{f}_i = \mathbf{R}\boldsymbol{\tau} \end{aligned}$$

Likewise, using the fact that $\mathbf{R}\mathbf{R}^\top = \mathbf{I}$, the new inertia matrix becomes

$$\begin{aligned} \mathbf{I}'_N &= \sum_i \|\mathbf{x}'_i - \boldsymbol{\mu}'\|^2 \mathbf{I} - (\mathbf{x}'_i - \boldsymbol{\mu}')(\mathbf{x}'_i - \boldsymbol{\mu}')^\top \\ &= \sum_i \|\mathbf{x}_i - \boldsymbol{\mu}\|^2 \mathbf{I} - (\mathbf{R}\mathbf{x}_i - \mathbf{R}\boldsymbol{\mu})(\mathbf{R}\mathbf{x}_i - \mathbf{R}\boldsymbol{\mu})^\top \\ &= \sum_i \mathbf{R} \|\mathbf{x}_i - \boldsymbol{\mu}\|^2 \mathbf{I} \mathbf{R}^\top - \mathbf{R}(\mathbf{x}_i - \boldsymbol{\mu})(\mathbf{x}_i - \boldsymbol{\mu})^\top \mathbf{R}^\top \\ &= \mathbf{R} \left(\sum_i \|\mathbf{x}_i - \boldsymbol{\mu}\|^2 \mathbf{I} - (\mathbf{x}_i - \boldsymbol{\mu})(\mathbf{x}_i - \boldsymbol{\mu})^\top \right) \mathbf{R}^\top \\ &= \mathbf{R}\mathbf{I}_N\mathbf{R}^\top \end{aligned}$$

For angular velocity, we have

$$\boldsymbol{\omega}' = \mathbf{C}\mathbf{I}_N'^{-1}\boldsymbol{\tau}' = \mathbf{C}\mathbf{R}\mathbf{I}_N^{-1}\mathbf{R}^\top\mathbf{R}\boldsymbol{\tau} = \mathbf{C}\mathbf{R}\mathbf{I}_N^{-1}\boldsymbol{\tau} = \mathbf{R}\boldsymbol{\omega}$$

Lastly, the updated coordinates become

$$\begin{aligned} \mathbf{x}_i^{\text{new}'} &= \mathbf{x}'_i + c_1\boldsymbol{\omega}' \times \mathbf{x}'_i + c_2\boldsymbol{\omega}' \times (\boldsymbol{\omega}' \times \mathbf{x}'_i) \\ &= \mathbf{R}\mathbf{x}_i + c_1(\mathbf{R}\boldsymbol{\omega} \times \mathbf{R}\mathbf{x}_i) + c_2(\mathbf{R}\boldsymbol{\omega} \times (\mathbf{R}\boldsymbol{\omega} \times \mathbf{R}\mathbf{x}_i)) \\ &= \mathbf{R}\mathbf{x}_i + c_1\mathbf{R}(\boldsymbol{\omega} \times \mathbf{x}_i) + c_2\mathbf{R}(\boldsymbol{\omega} \times (\boldsymbol{\omega} \times \mathbf{x}_i)) \\ &= \mathbf{R}\mathbf{x}_i^{\text{new}} \end{aligned}$$

Therefore, NERE layer is equivariant under rotation. \square

B. Experimental Details

Model hyperparameters. In the small molecule case, our model has two components: molecular graph encoder (MPN) and frame-averaging encoder. For the MPN part, we use the default hyperparameter from Yang et al. [34]. For the other encoder, we set hidden layer dimension to be 256 and try encoder depth $L \in \{1, 2, 3\}$ and distance threshold $d \in \{5.0, 10.0\}$. In the antibody case, we try encoder depth from $\{1, 2, 3\}$ and distance threshold $d \in \{10.0, 20.0\}$. In both cases, we select the hyperparameter with the best Pearson correlation on the validation set.

Docking protocol. For Autodock Vina, we use its default docking parameters with docking grid dimension of 20Å, grid interval of 0.375Å, and exhaustiveness of 32. For ZDOCK, we mark antibody CDR residues as ligand binding site and generate 2000 poses for each antibody-antigen pair. We re-score those 2000 poses by ZRANK2 and select the best candidate.

Additional analysis. Figure 6 shows how our model performance changes given different levels of docking error. We divide the test set into six groups based on their docking error (RMSD between docked and crystal ligand structure) and report the pearson correlation between predicted for each group. We observe that the performance difference is very small when docking RMSD is small (small molecules: 0-3Å, antibodies: 0-10Å). When docking RMSD is very large (over 50Å), the Pearson correlation becomes even negative. Overall, these results indicate that our model is robust to small docking error but performs much worse when there is significant docking error.

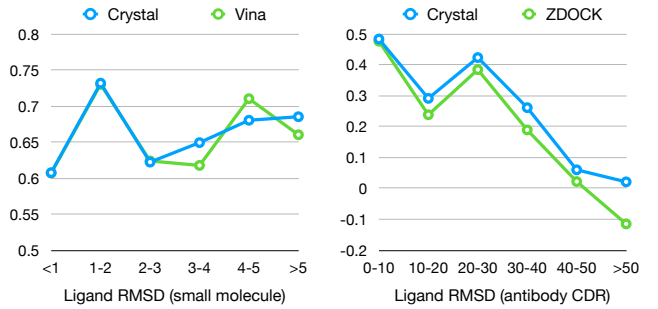


Figure 6. Model performance under different levels of docking error (left: small molecules; right: antibodies). Y-axis stands for Pearson correlation.